RSC Advances

ROYAL SOCIETY OF CHEMISTRY

www.rsc.org/advances

A fluorescence active gold nanorod-quantum dots core-satellite nanostructure for sub-attomolar tumor marker biosensing

Xiaoling Wu, Fengli Gao, Liguang Xu, Hua Kuang*, Libing Wang, Chuanlai Xu

The accurate monitoring of trace cancer biomarkers is crucial for the early diagnosis of cancer. In the present study, we constructed a gold nanorod-quantum dots core-satellite assembly using a PSA-aptamer and its complementary DNA and developed an ultrasensitive fluorescence-aptasensor for the detection of prostate specific antigen (PSA) by monitoring fluorescence intensity. The limit of detection (LOD) for PSA was 0.029 aM, with an excellent linear range from 0.1 aM to 10 aM. This super-sensitive aptasensor was demonstrated to be robust in the analysis of human serum samples, and shows great potential for early cancer diagnosis and therapy.

State Key Lab of Food Science and Technology, School of Food Science and Technology, Jiangnan University, Wuxi, JiangSu, 214122, PRC. E-mail: kuangh@jiangnan.edu.cn; Tel: 0510-85329076

1. Introduction

Early diagnosis of cancer is very important for therapy, and has recently attracted considerable research interest. However, the accurate detection of cancer biomarkers for early diagnosis is a global challenge, due to the trace amounts of these protein biomarkers[1]. Prostate specific antigen (PSA), a proteolytic enzyme, is mainly produced by prostate epithelial cells and is a significant tumor marker for the detection of prostate cancer[2-4]. The normal threshold value for PSA is lower than 4 ng/mL in serum, but there is still a significant risk of suffering prostate cancer in postoperative patients at much lower concentrations of PSA[5,6]. Therefore, it is necessary to monitor trace levels of PSA for the early diagnosis of prostate cancer.

Recently, multiple methods have been reported for the quantitative detection of PSA, including enzyme-linked immunosorbent assay (ELISA)[7], electrochemistry[8,9], Surface Enhanced Raman Scattering (SERS)[1,10], plasmonic circular dichroism (CD)[11,12], and others[13-15]. Despite the efforts made to accurately detect PSA, these methods lack either sufficient sensitivity, are time-consuming, or involve complicated fabrication steps and expensive equipment.

Fluorescent nanomaterials and their assemblies are a research hotspot, due to their wide application in the fields of fluorescence imaging, bio-analysis in vitro and vivo and clinical diagnosis[16-19]. In particular, semiconductor quantum dots (QDs) have attracted the attention of researchers and scientists, due to their narrow emission spectra and good fluorescent stability[20,21]. Studies have demonstrated that the fluorescence of QDs can be quenched or recovered by the assembly and disassembly of nanoassemblies comprised of QDs and noble metal nanoparticles[22,23]. In the present study, we fabricated a gold nanorod QDs (AuNR-QDs) core-satellite biosensor, using

a PSA-aptamer and its complementary DNA, for trace detection of PSA by monitoring fluorescence intensity.

2. Experimental sections

2.1 Materials

Thiolated DNA and amino-modified DNA oligonucleotides purified by high performance liquid chromatography (HPLC) were purchased from Shanghai Sangon Biological Engineering Technology & Services Co., Ltd. (Shanghai, China) and suspended in TE buffer at a final concentration of 100 μM.

Carboxyl-modified CdSe@ZnS core/shell QDs were purchased from Wuhan Jiayuan Quantum Dots Co., Ltd. (Wuhan, China). The deionized water was prepared using a Milli-Q device (18.2 M Ω, Millipore, Molsheim, France). All chemicals mentioned in this work were manufactured by Sigma-Aldrich. The relevant DNA sequences for PSA detection were as follows[10,11]:

PSA-aptamer sequence: 5'-SH-ATTAAAGCTCGCCATCAAATAGC-3'

PSA-complementary sequence: 5'-NH_2- TTTTTTGCTATTTGATGG-3'

The detailed control DNA sequences of the oligonucleotides are as follows:

Thrombin aptamer: 5'-HS-TTTTTGGTTGGTGTGGTTGG-3'

Thrombin - complementary sequences: 5'- NH_2-TTTTTTTAATTATATTAA-3'

2.2 Apparatus

Fluorescence spectra were measured using a HITACHI F-7000. A transmission electron microscope (TEM, JEOL JEM-2100) was employed to obtain images at an operating acceleration voltage of 200kV. The UV-vis spectra were obtained using a UNICO 2100PC UV/vis spectrophotometer. All glassware was soaked in aqua regia for 12 hours before use.

2.3 Synthesis of gold nanorods

Synthesis of gold seeds: 2.5 mL of 0.5 mM hydrogen tetrachloroaurate ($HAuCl_4$) and 2.5 mL of 0.2 M hexadecyltrimethylammonium bromide (CTAB) were mixed evenly followed by the addition of 0.3 mL of 0.01 M fresh sodium borohydride ($NaBH_4$) and stirred vigorously for 3 minutes.

Synthesis of AuNRs: 0.15 mL of 4 mM silver nitrate ($AgNO_3$) and 5 mL of 1 mM $HAuCl_4$ were added to 5 mL of 0.2 M CTAB, and then 70 μL of 0.0788 M ascorbic acid was added to the solution, which turned colorless when stirred. Following the addition of 12 μL of synthesized gold seeds, the AuNRs were obtained by bathing in 28°C water for 1 hour[24]. The AuNRs were then re-dispersed in 5 mM CTAB and stored at ambient temperature.

2.4 Gold nanorod modification

1 mL of AuNRs was centrifuged twice at the speed of 7300 rpm for 10 minutes and then resuspended and concentrated 10-fold in 5 mM CTAB solution. The PSA-aptamer was then added to the AuNRs with a molar ratio of DNA to AuNR of 300. The mixture was incubated for 12 hours at room temperature with gentle shaking. The conjugate was then collected and centrifuged twice (7500 rpm, 15 minutes), and the AuNR-DNA conjugate was obtained.

2.5 QDs modification

QDs were functionalized with amino-modified DNA using carbodiimide chemistry[25]. Briefly, QDs were diluted 200 times with water. 1-(3-Dimethylaminopropyl)-3-ethylcarbodiimide hydrochloride (EDC),

N-hydroxysuccinimide (NHS) and QDs were reacted at a molar ratio of 1000:1000:1 for 2 hours in water without light. The functionalized QDs were ultra-filtered (30 k molecular weight cutoff) and hybridized with amino-modified DNA (2 μL, 100 μM) in phosphate buffer (pH=7.5) for 3 hours. The QDs-DNA conjugates were obtained and were purified by ultrafiltration (30 k molecular weight cutoff).

2.6 Gold nanorod-QDs core-satellite assembly

To ensure the assembly yield, the functionalized AuNRs and QDs were mixed in 1×TBE buffer with 50 mM NaCl, 50 mM $Mg(NO_3)_2$ and 0.01% SDS and hybridized for 12 hours at room temperature[26,27]. The assemblies were centrifuged twice at 4500 rpm for 15 minutes. The supernatants were removed, and the pellet was re-suspended in water. High yield AuNR-QDs core-satellite assemblies were obtained.

2.7 Detection of PSA

In order to detect the target, PSA was added to the solution of functionalized AuNRs and QDs and mixed at final concentrations of 0 aM, 0.1 aM, 0.2 aM, 0.5 aM, 1 aM, 2 aM, 5 aM, and 10 aM, respectively. The fluorescence intensity was measured following incubation for 12 hours.

3. Results and Discussion

3.1 Establishment of the core-satellite biosensor

To fabricate the AuNR-QDs core-satellite assembly, the coupling ratios of aptamer and complementary DNA to AuNRs and QDs, and the molar ratio of these two functionalized nanomaterials should be well designed[10,27,28]. In this research, the molar ratio of DNA to AuNRs, and DNA to QDs was 300 and 2, respectively. The molar

ratio of AuNRs and QDs was kept as 1:80. Following DNA hybridization, the conjugated AuNRs and QDs were self-assembled to the core-satellite nanostructures. Scheme 1 shows the process of assembling the core-satellite biosensor for the detection of PSA. Initially, the AuNRs and QDs were coupled with the PSA-aptamer and PSA-complementary separately. When the reaction time was increased, more QDs combined with the AuNRs leading to the formation of core-satellite assemblies (Fig. 1 and Fig. S1). AuNR-QDs core-satellite assemblies were constructed in the absence of PSA. When PSA was added, the aptamer competitively bound to PSA, resulting in a low yield of the AuNR-QDs core-satellite assembly.

The prepared AuNRs, QDs and core-satellite assembly were characterized by TEM (Fig. S2). As shown in the TEM images (Fig. 1), when increasing concentrations of PSA were added, fewer QDs bound to the AuNRs, and higher fluorescence intensity was observed due to an increased number of free QDs in solution. The dynamic light scattering measurements (DLS) were also performed. As showed in Fig. S3, the hydrodynamic diameter of the Au NR-QDs core-satellite assemblies gradually decreased with the increasing concentration of PSA target. UV-vis spectra were adopted to monitor AuNR-DNA1, QDs-DNA2 and AuNR-QDs core-satellite assemblies (Fig. S4). The longitudinal surface plasmon peak of AuNR-QDs core-satellite assemblies shifted toward the blue part of the spectrum, which was consistent with earlier reports[28,29]. There was no observable shift at the transverse band, which may have been due to low coupling of the transverse plasmon dipoles[30].

As shown in Fig. S5, the emission wavelength of QDs was 600 nm. We recorded fluorescence intensity at 600 nm to establish a calibration curve of PSA concentration and corresponding fluorescence intensity. Due to large-scale AuNR-QDs core-satellite assemblies in the sample, the fluorescence of QDs was quenched which can be seen in Fig. 2(A) with 0 aM of PSA. When PSA was simultaneously added to the solutions,

fluorescence of the solution recovered as some of the QDs were released from the assemblies. Before the PSA detection, we tested the stability of the developed biosensor. As showed in Figs. S6 and S7, the AuNR-QDs core-satellite assemblies were stable in suspension for more than 24h with or without addition of PSA target. And the fluorescence intensity also remained unchanged in the tested pH values (pH 7.0-8.5, Figs. S8 and S9) with or without addition of PSA target, indicating the good stability of the proposed biosensor. A calibration curve of the logarithmic concentration of PSA as the x axis and fluorescent intensity as the y axis was plotted. From the results shown in Fig. 2B, the established method displayed a good linear range from 0.1 aM to 10 aM with an excellent correlation coefficient of R^2=0.998. The limit of detection (LOD) was calculated to be 0.029 aM, which was more sensitive than immunosensors or electrochemical sensors (Table S1), and was comparable to the most sensitive biosensor for PSA detection reported so far[12]. This sensitivity was probably due to the linear response of the fluorescence signal with the conformational changes of the nanoassembly, high affinity of the aptamer, and good signal to noise ratio.

3.2 Selectivity of the core-satellite assembly in PSA detection

To confirm the selectivity of this method, other targets were added to prepared samples and their fluorescence intensity was measured under the same conditions as those for PSA. In the control, no targets were added to the sample. Vascular endothelial growth factor (VEGF), mucin-1, thrombin, immunoglobulin G (Ig G), bull serum albumin (BSA) and alpha-fetoprotein (AFP) were detected at a final concentration of 50 aM and PSA was detected at 10 aM. These results were shown in Fig. 3 and the original spectra are shown in Fig. S10. The fluorescence recovered only

after the addition of PSA, while the other samples showed low fluorescence intensity, indicating the high specificity of this core-satellite assembly. In addition, we also added a control experiment, where the Au NR-QDs core-satellite assemblies were prepared using a DNA sequences that was not able to recognize the the target PSA protein (thrombin aptamer and its complementary sequence). As showed in Fig. S11, the fluorescence intensity of the assemblied Au NR-QDs core-satellite showed no obvious change with the increasing concentration of the PSA, which further indicated the high selectivity of the established biosensor.

3.3 Analysis of PSA in human serum samples

The reliability of the developed method was tested by analyzing PSA in real samples which were obtained from the Second Hospital in Wuxi, P.R.C. The PSA concentration was confirmed using the standard clinical diagnostic assay (ADVIA Centaur, Siemens). The original samples were diluted 10000 times and determined as shown in Table. S2 and Fig. S12. The results were almost consistent with the determined concentrations. Hence, this method is considered feasible and promising for clinical applications.

4. Conclusions

In summary, a fluorescence-aptasensor for the sub-attomolar detection of PSA was fabricated based on a AuNR-QDs core-satellite assembly. The established sensor showed accuracy in detecting PSA, with a LOD as low as 0.029 aM. The sensor also demonstrated good specificity and robustness in the analysis of complicated human serum samples. By replacing the aptamer, the developed fluorescence-aptasensor can

easily be expanded to detect other types of cancer biomarkers, which will open an avenue for the early diagnosis of cancers.

Acknowledgements

This work is financially supported by the National Natural Science Foundation of China (21522102, 21503095) and grants from Natural Science Foundation of Jiangsu Province, MOF and MOE (BK20150145, BX20151038, BK20140003, BE2013613, BE2013611).

References

1. L. Xu, W. Yan, W. Ma, H. Kuang, X. Wu, L. Liu, Y. Zhao, L. Wang, C. Xu, *Adv. Mater.,* 2015, **27**, 1706-1711.
2. P. E. Castle, *Lancet Oncol.,* 2015, **16**, 2-3.
3. J. Cuzick, M. A. Thorat, G. Andriole, O. W. Brawley, P. H. Brown, Z. Culig, R. A. Eeles, L. G. Ford, F. C. Hamdy, L. Holmberg, *Lancet Oncol*., 2014, **15**, 484-492.
4. I. M. Thompson, C. Chi, D. P. Ankerst, P. J. Goodman, C Tangen,. M. S. M. Lippman, M. S. P Lucia, H. L. arnes, C. A. Coltman, *J. Natl. Cancer Inst.,* 2006, **98**, 1128-1133.
5. C. S. Thaxton, R. Elghanian, A. D. Thomas, S. I. Stoeva, J.-S. Lee, N. D. Smith, A. J. Schaeffer, H. Klocker, W. Horninger, G. Bartsch, *Proc. Natl. Acad. Sci., U.S.A.* 2009, **106**, 18437-17442.
6. I. M. Thompson, D. P. Ankerst, C. Chi, M. S. Lucia, P. J. Goodman, J. J. Crowley, H. L. Parnes, C. A. Coltman, *JAMA-J AM MED ASSOC,* 2005, **294**, 66.
7. H. A. Ahmed, H. M. Azzazy, *Biosens. Bioelectron.,* 2013, **49**, 478-484.
8. K. Chuah, L. M. Lai, I. Y. Goon, S. G. Parker, R. Amal, J. J. Gooding, *Chem. Commun.,* 2012, **48**, 3503-3505.
9. D.-J. Kim, N.-E. Lee, J.-S. Park, I.-J. Park, J.-G. Kim, H. J. Cho, *Biosens. Bioelectron.* 2010, **25**, 2477.
10. W. Ma, H. Yin, L. Xu, X. Wu, H. Kuang, L. Wang, C. Xu, *Chem. Commun.,* 2014, **50**, 9737-9740.

11. L. Tang, S. Li, L. Xu, H. Kuang, L. Wang, C. Xu, W. Ma, *Acs. Appl. Mater. Inter.,* 2015, **7**, 12708-12712.
12. X. Wu, L. Xu, L. Liu, W. Ma, H. Yin, H. Kuang, L. Wang, C. Xu, N. A. Kotov, *J. Am. Chem. Soc.*, 2013, **135**, 18629-18636.
13. A. Dey, A. Kaushik, S. K. Arya, S. Bhansali, *J. Mater. Chem.,* 2012, **22**, 14763.
14. D. Liu, X. Huang, Z. Wang, A. Jin, X. Sun, L. Zhu, F. Wang, Y. Ma, G. Niu, A. R. Hight Walker, *ACS Nano,* 2013, **7**, 5568-5576.
15. Z. Wang, N. Liu, F. Feng, Z. Ma, *Biosens. Bioelectron.,* 2015, **70**, 98.
16. Y. Li, Y. Sun, J. Li, Q. Su, W. Yuan, Y. Dai, C. Han, Q. Wang, W. Feng, F. Li, *J. Am. Chem. Soc.,* 2015. **137**, 6407.
17. S. Wennmalm, J. Widengren, *J. Am. Chem. Soc.,* 2012, **134**, 19516-19519.
18. J. Yao, M. Yang, Y. Duan, *Chem. Rev.,* 2014, **114**, 6130.
19. W. Zhang, W. Liu, P. Li, H. Xiao, H. Wang, B. Tang, *Angew. Chem. Int. Ed.,* 2014, **126**, 12697.
20. W. C. Chan, S. Nie, *Science,* 1998, **281**, 2016-2018.
21. K. D. Wegner, N. Hildebrandt, *Chem. So*c. Rev., 2015. **44**, 4792-4834.
22. E. Oh, M.-Y. Hong, D. Lee, S.-H. Nam, H. C. Yoon, H.-S. Kim, *J. Am. Chem. Soc.,* 2005, **127**, 3270-3271.
23. Z. Zhu, J. Guo, W. Liu, Z. Li, B. Han, W. Zhang, Z. Tang, *Angew. Chem. Int. Ed.,* 2013, **125**, 13816.
24. B. Nikoobakht, M. A. El-Sayed, *Chem. Mater.,* 2003, **15**, 1957-1962.
25. W. Yan, L. Xu, C. Xu, W. Ma, H. Kuang, L. Wang, N. A. Kotov, *J. Am. Chem. Soc.,* 2012, **134**, 15114-15121.
26. L. Xu, C. Hao, H. Yin, L. Liu, W. Ma, L. Wang, H. Kuang, C. Xu, *J. Phys. Chem. Lett.,* 2013, **4**, 2379-2384.
27. L. Xu, H. Kuang, C. Xu, W. Ma, L. Wang, N. A. Kotov, *J. Am. Chem. Soc.,* 2012, **134**, 1699-1709.
28. X. Zhao, X. Wu, L. Xu, W. Ma, H. Kuang, L. Wang, C. Xu, *Biosens. Bioelectron.,* 2015, **66**, 554-558.
29. J. Feng, X. Wu, W. Ma, H. Kuang, L. Xu, C. Xu, *Chem. Commun.,* 2015, **DOI**: 10.1039/C5CC05255F.
30. P. K. Jain, S. Eustis, M. A. El-Sayed, *J. Phys. Chem. B,* 2006, **110**, 18243-18253.

Captions:

Scheme 1. Scheme for fluorescence detection of PSA based on AuNR-QDs core-satellite assembly.

Fig. 1 TEM images of Au NR-QDs core-satellite assemblies with different concentration of PSA. (A) 0 aM, (B) 0.1 aM, (C) 0.5 aM, (D) 1 aM, (E) 5 aM, and (F) 10 aM.

Fig. 2 PSA detection based on fluorescence with Au NR-QDs core-satellite assemblies. A) Fluorescence spectra of PSA detection. B) Standard curve for PSA detection with corresponding fluorescence intensities at 600 nm.

Fig. 3 The bar chart corresponding with fluorescence intensity of the assemblies toward different targets.

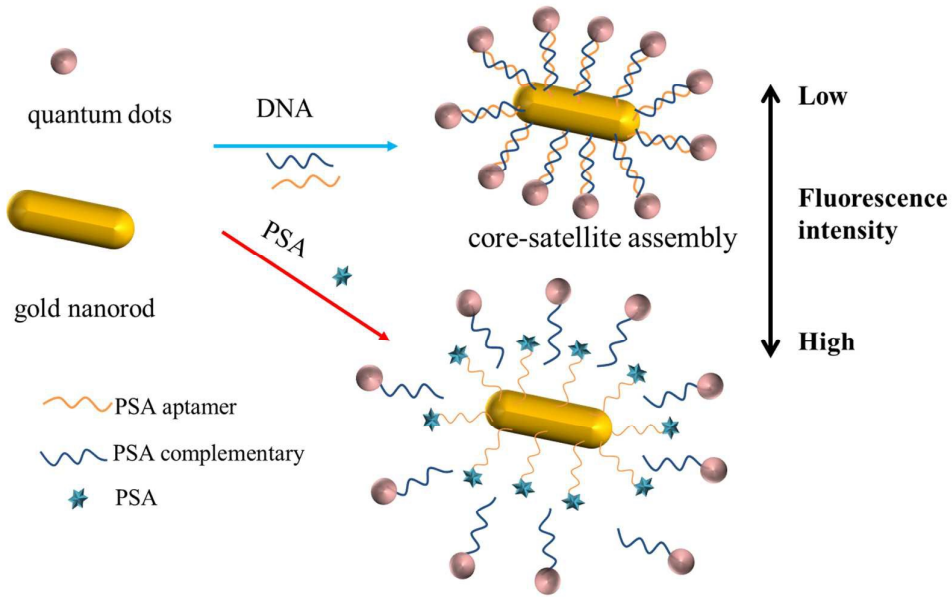

Scheme 1 Scheme for fluorescence detection of PSA based on AuNR-QDs core-satellite assembly.

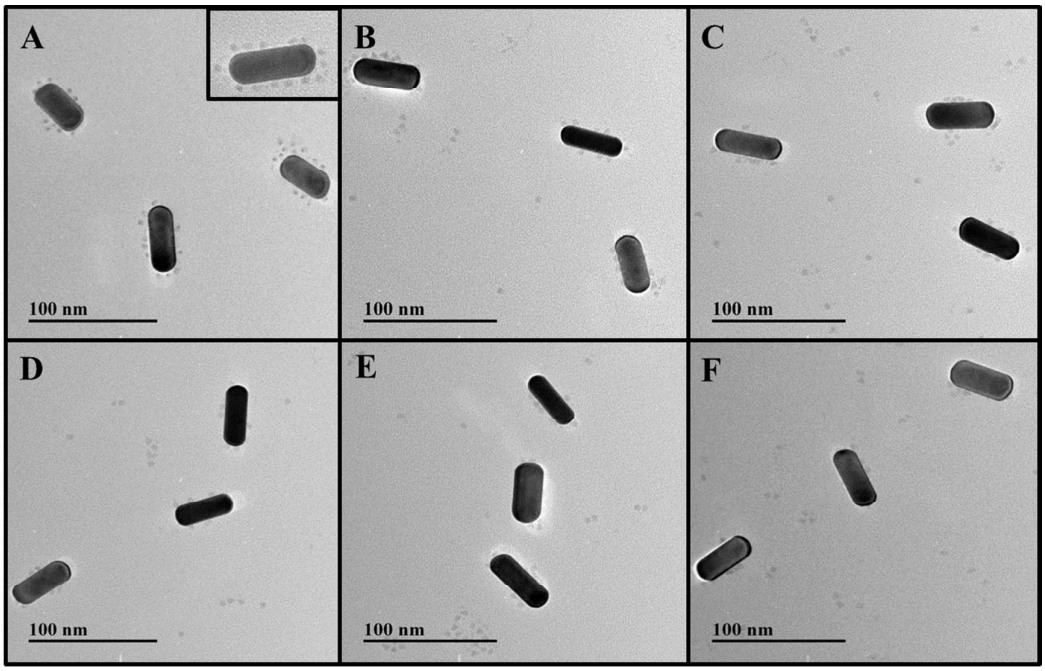

Fig. 1 TEM images of Au NR-QDs core-satellite assemblies with different concentration of PSA. (A) 0 aM, (B) 0.1 aM, (C) 0.5 aM, (D) 1 aM, (E) 5 aM, and (F) 10 aM.

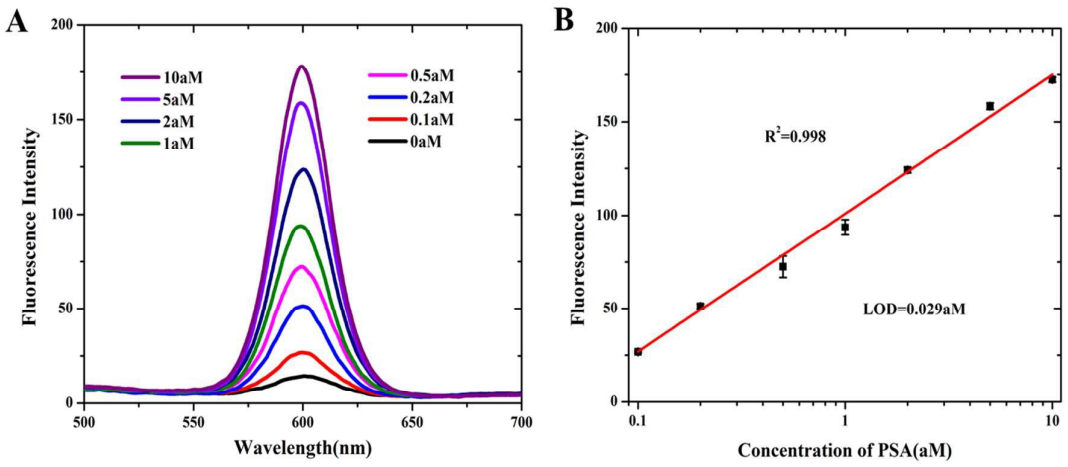

Fig. 2 PSA detection based on fluorescence with Au NR-QDs core-satellite assemblies. A) Fluorescence spectra of PSA detection. B) Standard curve for PSA detection with corresponding fluorescence intensities at 600 nm.

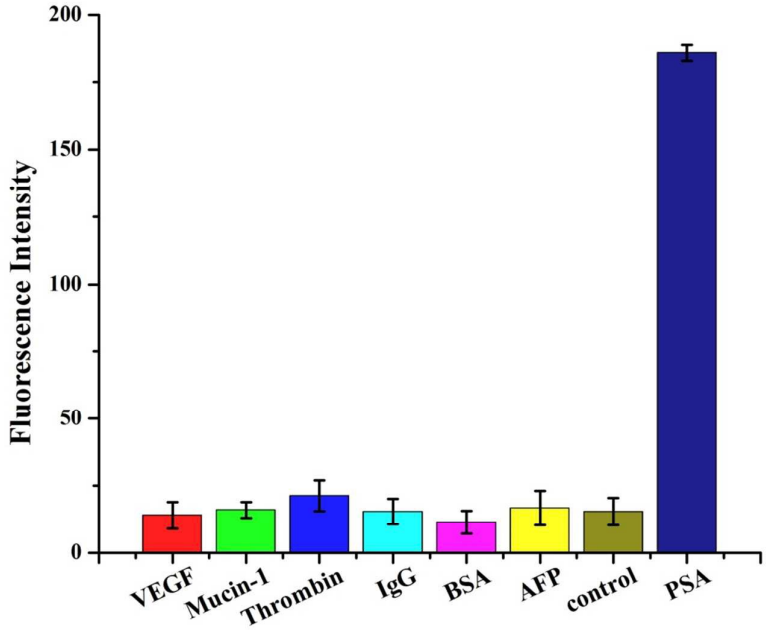

Fig. 3 The bar chart corresponding with fluorescence intensity of the assemblies toward different targets.